Long-range temperature-controlled transport of ultra-cold atoms with an accelerated lattice

L Absil, Y Balland, Franck Pereira dos Santos

New Journal of Physics
The open access journal at the forefront of physics

Deutsche Physikalische Gesellschaft DPG IOP Institute of Physics

PAPER • OPEN ACCESS

Long-range temperature-controlled transport of ultra-cold atoms with an accelerated lattice

To cite this article: L Absil *et al* 2023 *New J. Phys.* **25** 073010

IOP Publishing New J. Phys. 25 (2023) 073010 https://doi.org/10.1088/1367-2630/ace3ea

New Journal of Physics
The open access journal at the forefront of physics

Deutsche Physikalische Gesellschaft DPG
IOP Institute of Physics

Published in partnership with: Deutsche Physikalische Gesellschaft and the Institute of Physics

OPEN ACCESS

RECEIVED
10 March 2023

REVISED
15 June 2023

ACCEPTED FOR PUBLICATION
4 July 2023

PUBLISHED
17 July 2023

PAPER

Long-range temperature-controlled transport of ultra-cold atoms with an accelerated lattice

L Absil, Y Balland and F Pereira Dos Santos*

LNE-SYRTE, Observatoire de Paris, Université PSL, CNRS, Sorbonne Université, 61 avenue de l'Observatoire, Paris 75014, France
* Author to whom any correspondence should be addressed.

E-mail: franck.pereira@obspm.fr

Keywords: atom interferometry, quantum sensor, atom transport, Bloch oscillations

Abstract

We report our method for transporting ultracold atoms over macroscopic distances and trapping them back in a vertical mixed trap, consisting of the superposition of a vertical lattice and a transverse confinement beam. The transport is performed with Bloch oscillations allowing us to move up to 25% of a sub-micro-Kelvin atomic cloud on a distance of the order of 30 cm, without excessive heating and with an excellent control of its final position. The efficiency is lowered to about 10% after trapping them in the vertical mixed trap during extended times.

1. Introduction

The transport of clouds of cold atoms or Bose–Einstein condensates (BEC) from their production area to other areas of experimental interest has drawn much attention since first implementations in the 90s [1]. Various approaches have been considered, using magnetic or optical fields, depending on the desired specifications. Magnetic traps have proven to be a suitable solution for moving thermal clouds at temperatures above the micro-Kelvin range over long distances of tens of centimeters, but at the cost of heating up the sample [2–7]. On the other hand, trapping the atomic cloud in optical lattices has proven to be a solution of choice for precise displacement of single atoms over distances of the order of the centimeter [8, 9], for adiabatic centimeter-long transport of ultracold atoms [10], or fast transport of cold atoms in the decimeter range using Bessel beams [11]. Other solutions involving the use of a focus-tunable moiré lens [12], other optical systems of tunable-zoom [13] or optical tweezers [14] have also shown their interest to transport atomic cloud either on short distances with reasonably small heating or, on long distances, with more consequent warm-up of the atomic cloud and a weak confinement in the direction of transport.

In the experiment reported here, we aim at performing ultra-sensitive short range forces measurements, with a quantum sensor based on ^{87}Rb atoms trapped in an optical trap, consisting of a vertical shallow lattice $\lambda_{\mathrm{Verdi}} = 532$ nm overlapped with a transverse confinement potential $\lambda_{\mathrm{IR}} = 1064$ nm. In such a system, energy differences between adjacent lattice sites can be probed with a Ramsey-Raman interferometer [15] providing us a local measurement of the vertical force exerted on the atoms. The goal is to probe micrometer-range forces occurring between our atomic cloud and the surface of a mirror. Previous attempts at similar measures have shown the importance of preparing the sample away from the surface of the mirror in order to minimize any undesired adsorption of the atoms [16, 17]. Furthermore, the spatial resolution of the measurements is limited by the final size of the cloud in the vertical direction, perpendicular to the surface of the mirror, and by the accuracy of our control of the distance from the cloud to the mirror. We start with a cloud of a few micrometers [15]. To ensure an accurate control of the distance covered by the atoms and their vertical confinement throughout transport, we chose to transport them using a moving lattice [1, 10, 11].

We present here the outcomes of our experimental setup which enables the transportation of up to 25% of a sub-micro-Kelvin atomic cloud on a distance of the order of 30 cm, without inducing excessive heating and while maintaining control over its size and final position. We first provide a general overview of the experimental setup and of the main sources of loss expected, before reporting our results on the transport efficiency and the control of the atoms position.

2. Experimental setup

Figure 1(a) summarizes the main steps of the atom preparation. A two-dimensional magneto-optical-trap (2D-MOT) loads atoms in a three-dimensional magneto-optical trap (3D-MOT), which in turn loads a crossed dipole trap where evaporative cooling is performed down to a temperature of 300 nK and an atomic density of the order of 10^{12} atoms cm^{-3}. Then, atoms are launched upward and transported over 30 cm, up to the vicinity of the surface of the lattice mirror, where measurements are to be performed.

The elevator consists of the overlapping of two counterpropagating beams '*Bloch 1*' and '*Bloch 2*' whose frequency differences and intensities are tuned over time. Atoms are thus loaded in an accelerated or decelerated lattice of adjustable depth.

2.1. Setup

The Bloch beams are derived from a single external-cavity diode laser, which is split in two. Each beam is sent to a double pass acousto-optic modulator (AOM) before injecting a 2 W tapered amplifier (TA). Each amplified beam then passes through an other single pass AOM and then injects a polarization maintaining fiber. One fiber directs the first Bloch beam to the bottom of the experimental setup, where it enters the vacuum chamber, while the other fiber brings the second Bloch beam to the top. Finally, they are overlapped to counterpropagate along the vertical direction. This setup allows for modulating the frequency difference between the beams during the transport with the AOMs before the TAs, and their powers with the AOMs placed after the TAs.

2.2. Atoms in moving lattices

The periodic potential $U(z)$ resulting from the interference of the two counter-propagating beams '*Bloch 1,2*' of intensity $I_{1,2}$ is proportional to the local intensity experienced by the atoms $I(z) = 2I_0(1 + m\cos 2kz)$, where I_0 is the average intensity, m the ratio of the geometric and arithmetic means of the intensities of each beam and k is the modulus of the wavevector of the laser:

$$U(z) = \frac{U_0}{2}(1 + m\cos 2kz) \tag{1}$$

For a detuning Δ of the order of hundreds of GHz with respect to the D2 line of ^{87}Rb, the depth is $U_0 \sim \hbar\Gamma^2 I_0/(3\Delta I_s)$, where Γ and I_s are the natural linewidth and the saturation intensity of the transition. By imposing a frequency difference $\Delta\omega$ between the two Bloch beams, we then move the lattice potential with a velocity $v_{\mathrm{latt}} = \Delta\omega/2k$. This allows us to coherently accelerate the atoms through Bloch oscillations [18], each oscillation imparting a $2\hbar k$ momentum transfer to the atoms.

For the measurements presented here, the detuning Δ is set to -250 GHz. For maximum powers around 50 mW in the two beams, with identical waists of 400 μm, we calculate a maximum depth around 150 E_r, with $E_r = \frac{\hbar^2 k^2}{2m_{Rb}}$ the recoil energy. This is in reasonable agreement with a determination of the depth based on Raman–Nath diffraction, where from the measurement of the populations in the diffracted orders as a function of duration of a square pulse performed before the transport, we deduced a maximum depth of about 110 E_r.

Figure 2 illustrates the typical sequence of transport. The atoms are first adiabatically loaded into the lattice, by increasing the depth from 0 to U_{acc} in 600 μs while ramping the frequency difference between the two beams by 25 MHz s^{-1}. This corresponds to accelerating the lattice by g.

Then, the lattice is accelerated upwards over 6 ms at a fixed lattice depth U_{acc}. The chirp of the frequency difference between the beams corresponds to N_{acc} Bloch oscillations. After a certain transport time at constant velocity, where the lattice potential may be reduced, the atoms are decelerated at a depth U_{dec} with N_{dec} Bloch oscillations. The atoms are then adiabatically released by reducing the lattice potential down to zero in 600 μs. They are then trapped in the mixed trap illustrated in figure 1, where force measurements are to be performed. This mixed trap consists of the superposition of a green lattice, which we turn on 400 μs before the end of the adiabatic release, and an IR transverse confinement beam, which we keep at full power of 2 W during the transport and the recapture in the mixed trap.

Between the acceleration and deceleration, we keep the transport lattice at a depth U_{ff} in order to keep the atoms vertically and transversally confined. Additional transverse confinement is also provided by the IR laser at 1064 nm. Its waist, of the order of 200 μm is placed at the target position of the atoms, near the surface of the lattice mirror.

2.3. Sources of loss

Common sources of loss during the transport with Bloch oscillations are spontaneous emission and non-adiabatic losses. We suffer from two sources of spontaneous emission. The first comes from the

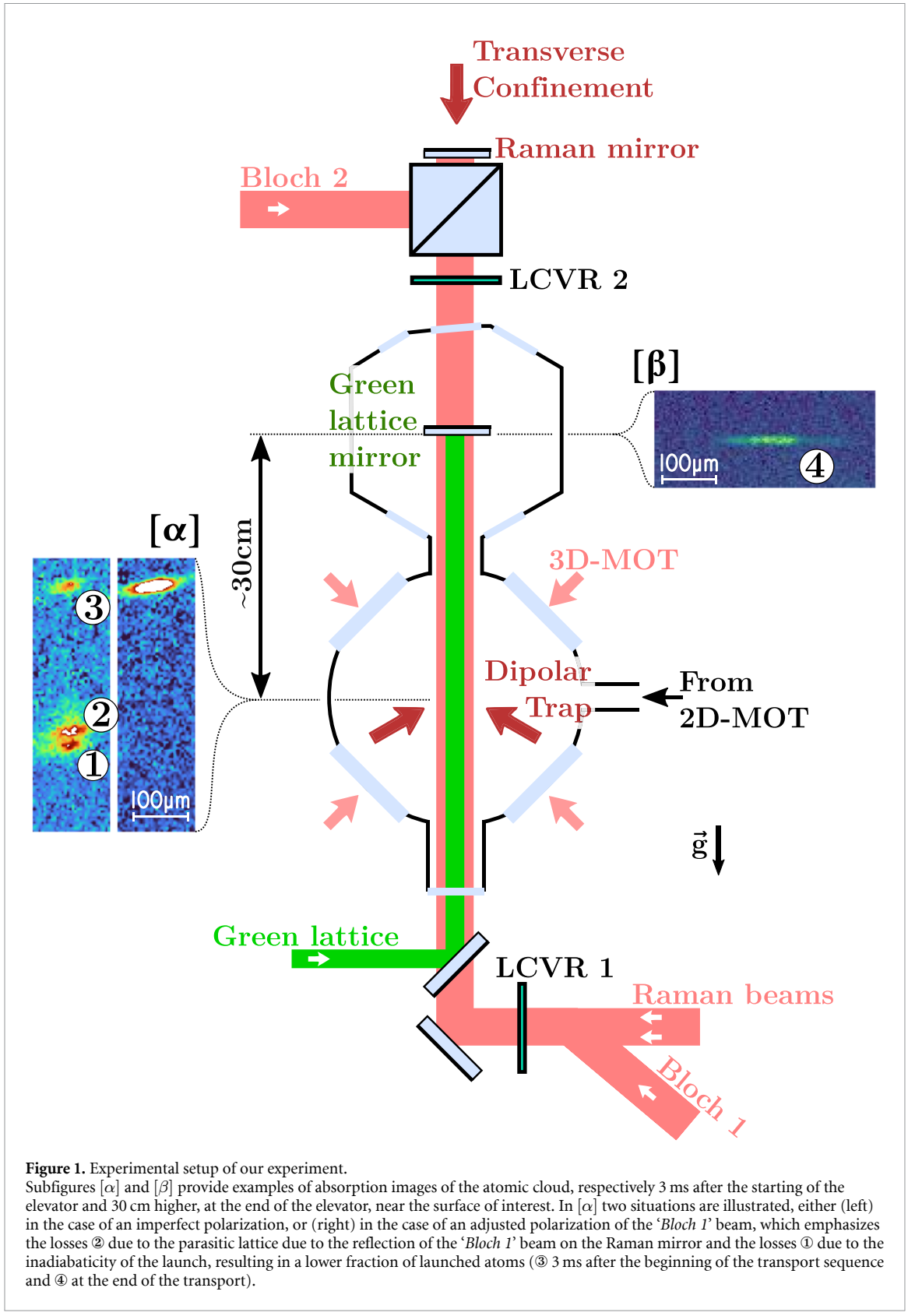

Figure 1. Experimental setup of our experiment.
Subfigures [α] and [β] provide examples of absorption images of the atomic cloud, respectively 3 ms after the starting of the elevator and 30 cm higher, at the end of the elevator, near the surface of interest. In [α] two situations are illustrated, either (left) in the case of an imperfect polarization, or (right) in the case of an adjusted polarization of the '*Bloch 1*' beam, which emphasizes the losses ② due to the parasitic lattice due to the reflection of the '*Bloch 1*' beam on the Raman mirror and the losses ① due to the inadiabaticity of the launch, resulting in a lower fraction of launched atoms (③ 3 ms after the beginning of the transport sequence and ④ at the end of the transport).

monochromatic Bloch beams detuned by Δ at a rate of order of $P_{sp} \sim U_0\Gamma/\hbar\Delta$ and leads to losses that increase with the duration of the transport. A second one comes from the amplified spontaneous emission near resonance of the tapered amplifiers, which we efficiently filter using narrow bandwidth (of order of ~150 GHz) interference laser line filters. This in turn forces us to use large enough detunings.

For their efficient transport with Bloch oscillations, atoms have to be initially loaded and then to remain in the lower band of the moving lattice. The adiabaticity of the acceleration process restricts accelerations to

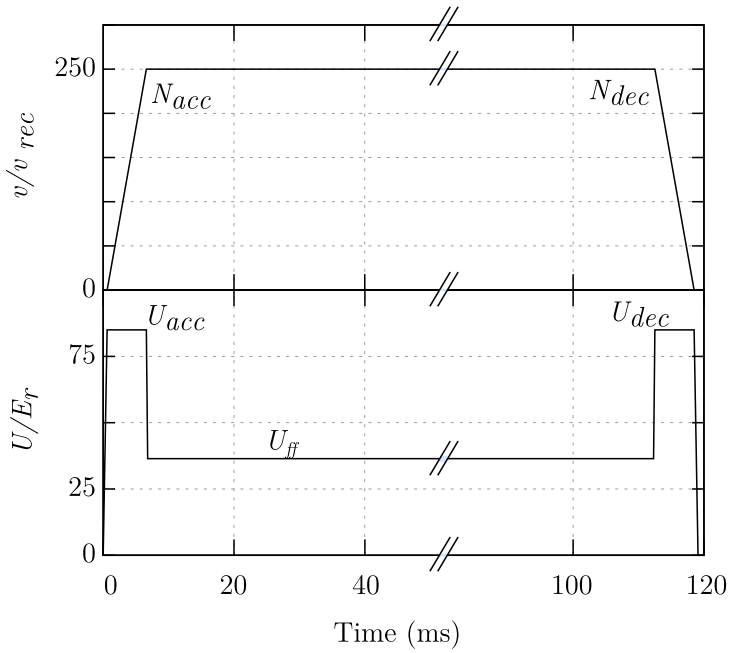

Figure 2. Optimal transport sequence. The velocity v and the lattice depth U during the different phases of the elevator are expressed in terms of recoil velocity $v_{\mathrm{rec}} = \hbar k/m$ and recoil energy E_r. The velocity v is kept constant in between the acceleration and deceleration phases, during which the atoms experience N_{acc} and N_{dec} Bloch oscillations respectively.

below a critical value, which, in the weak binding limit, can be deduced from the Landau–Zener formula [18]. The larger the depth, the larger this critical acceleration, and generally losses decrease with decreasing accelerations, and thus longer transport durations, by contrast with losses by spontaneous emission. This calls for a compromise between these two sources of losses. Note that for depths below 20 E_r, resonances between the energy bands also reduces the efficiency in certain acceleration ranges [19, 20].

Finally, specific to our optical setup, a last source of loss is due to small fractions of the '*Bloch 1*' beam that retroreflects on the green lattice and Raman mirror. These create additional static lattices, in which a fraction of the atoms, can be trapped as displayed in figure 1(α). To minimize them, the green lattice mirror has been designed to have a low reflectivity at 780 nm (0.6%), and the polarization beam splitter prevents the '*Bloch 1*' beam from being reflected onto the Raman mirror. In practice, a residual reflection is minimized by carefully adjusting the polarization of the beam.

2.4. Detection

Two different detection schemes are used to evaluate the performance of our transport system. We use in-situ absorption imaging with a CCD camera model Pixelfly from PCO company in the bottom chamber, and both absorption imaging or fluorescence detection with a deeply cooled EM-CCD camera model C9100 from Hamamatsu company in the top chamber. This allows us to measure the number of atoms in the $|F = 2\rangle$ state and their temperature in both chambers. In-situ fluorescence imaging in the top chamber allows to measure with a better atom detectivity but without much spatial resolution the number of atoms in each of the $|F = 1\rangle$ and $|F = 2\rangle$ states.

3. Results

To optimize the launch efficiency of the atoms, we start by imaging in the bottom chamber their position 3 ms after their acceleration. Figure 1(α) left displays an absorption imaging picture featuring three different groups of atoms: ③ launched, ② trapped in a parasitic lattice due to reflection of the '*Bloch 1*' beam on the Raman mirror, and ① untrapped and in free fall. By adjusting the polarization of the '*Bloch 1*' beam, we eliminate the loss of atoms in both groups ① and ②, which results in a single group of atoms as displayed at the right. We then increase the number of Bloch oscillations until the atoms can reach the top chamber, where we obtain a first signal (similar to the one in figure 1(β)). We next optimize the durations of the different transport phases, keeping the transport distance constant. This initial optimization results in durations of 6 ms for both acceleration and deceleration phases, with 250 Bloch oscillations at the acceleration as displayed in figure 2. We optimize afterwards the other parameters, such as the power of the

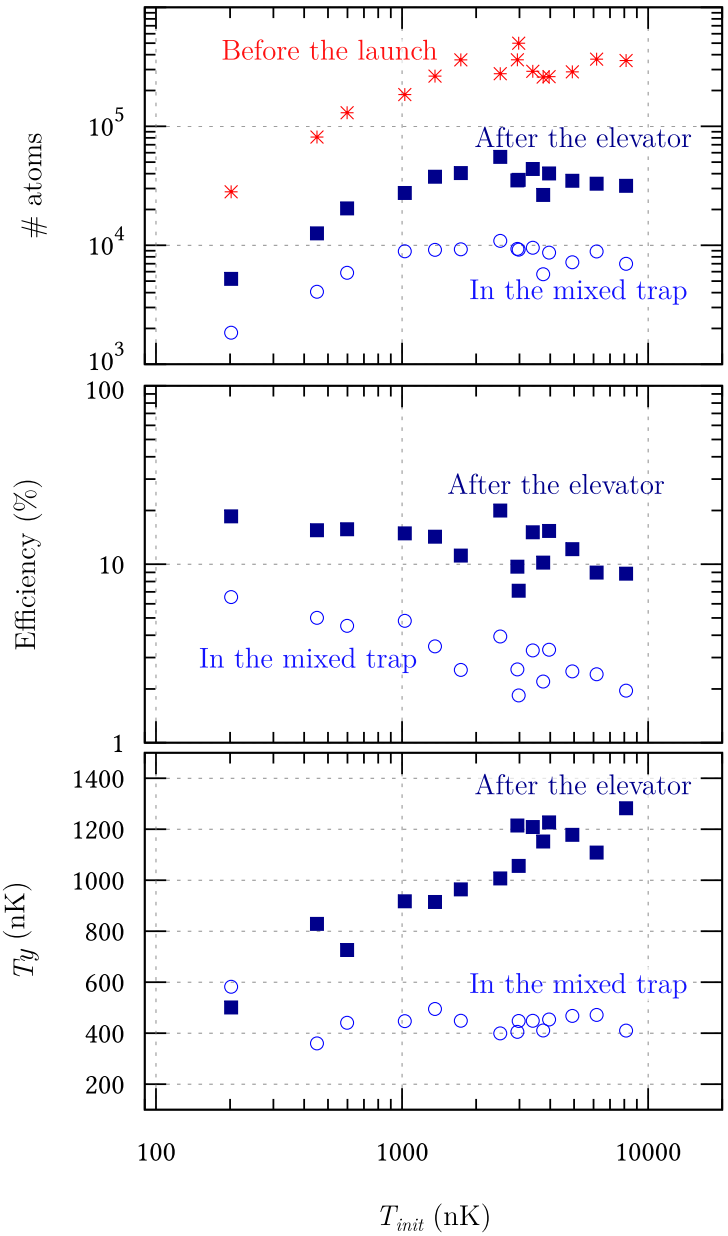

Figure 3. Top figure: influence of the initial temperature T_{init} of the cloud (at the end of the evaporative cooling and right before the launch) on the number of atoms at the end of the evaporation (red stars), at the end of the transport (full squares) and after 1 s in the mixed trap (open circles).
Center figure: corresponding transport and capture efficiencies.
Bottom figure: corresponding temperatures T_y in the vertical direction.

'*Bloch*' beams or the temperature of the atoms before the transport. We finally vary back the duration and number of Bloch oscillations without much improvement.

We illustrate in figure 3 the influence of the initial temperature of the atoms both on the number and the temperature of the atoms after their transport over the 30 cm distance and after their trapping in the mixed trap described above. We find that the efficiency of both processes reduces when increasing the initial temperature. We attribute this for one to the velocity selectivity of the acceleration process, that works best for atoms moving at subrecoil velocities in the frame of the lattice, and for the other to the shallow depth of the mixed trap. Note that the efficiency is not the only relevant parameter when it comes to selecting the most appropriate parameters for our transport system. It can be of interest for instance to work either with high initial temperatures, which, despite the lower efficiency, leads indeed to larger number of transported atoms, or with lower initial temperature, which leads to smaller sizes at the end. These relevant parameters actually depend on the details of the evaporative cooling stage, where temperature, number of atoms and initial size are correlated.

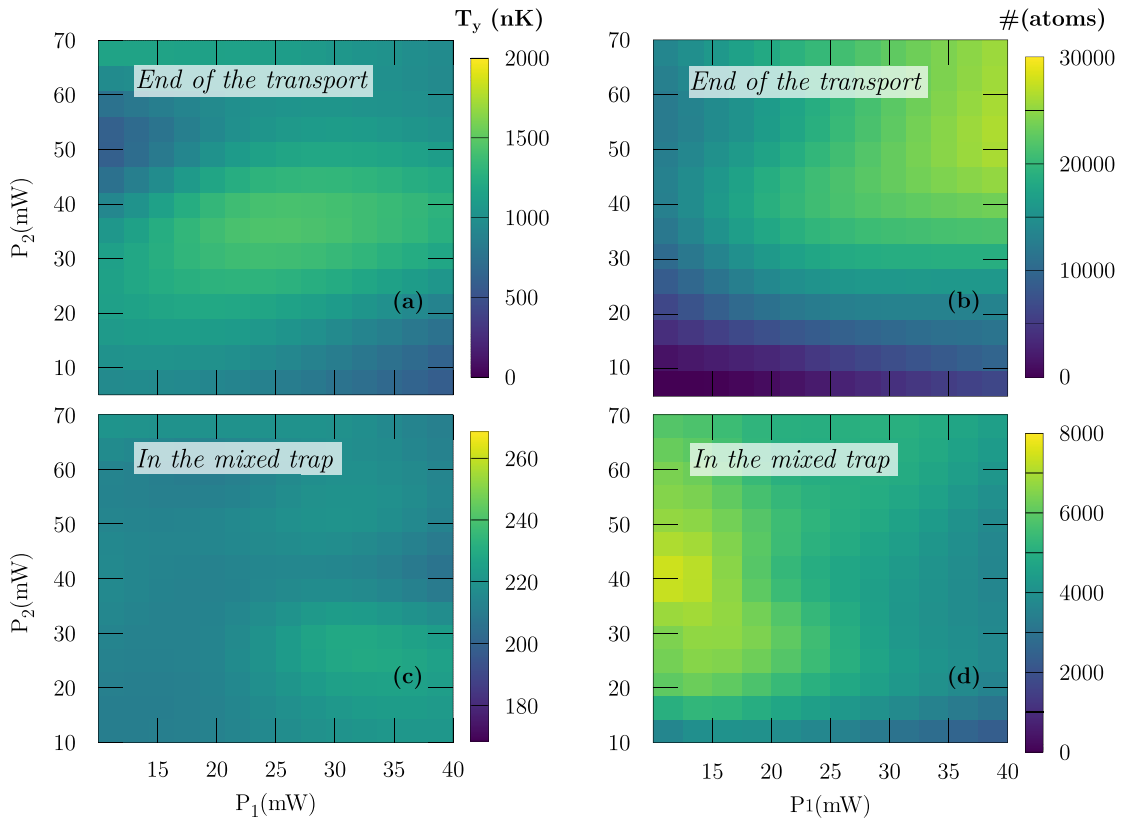

Figure 4. Influence of the powers $P_{1,2}$ in the Bloch beams (1 and 2 respectively) on the number of atoms and temperature in the vertical direction T_y, either at the end of transport ((a) and (b)), or after their recapture in the mixed trap (during 1 s) ((c) and (d)).

The influence of the powers in the Bloch beams during the transport is illustrated in figure 4(a). The larger the powers, the higher the depth, and the more efficient is the transport. However, for an efficient subsequent loading in the mixed trap, the power in the '*Bloch 1*' beam needs to be reduced, as shown in figure 4(c), which displays the number of atoms in the mixed trap after a trapping time of 1 s. We attribute this feature to the presence of residual parasitic static lattices, related to the reflection of the '*Bloch 1*' beam on the Raman and green lattice mirrors.

Other parameters have also been varied without much improvement. We can for instance mention the influence of the depth used during the transport (U_{ff}). While decreasing the depth at this stage reduces in principle losses due to spontaneous emission, it comes at the price of a large decrease in the number of transported atoms, which we attribute to the reduction in the transverse confinement. Therefore this depth is kept constant, as high as during the acceleration and deceleration phases, for all the measurements presented here.

The position stability of the cloud after the transport is a key objective for our experimental setup. To check its evolution over time, we alternate absorption imaging measurements of the cloud before and after the transport. The corresponding Allan standard deviations of those two signals and of their difference are plotted in figure 5.

A larger measurement noise is observed for the position before the launch in the bottom chamber, which we attribute to the larger size of the cloud, whose center position has been measured after a 6 ms thermal expansion in free fall, and to the larger readout noise of the bottom camera compared to the top one.

On both positions of the cloud, we observe a bump on the Allan deviation, occurring around 200 s. This perturbation is correlated with the temperature cycles of our air conditioning system and is actually eliminated when calculating the difference of the two signals, since the Allan deviation of this difference averages down to about 100 nm at 1000 s. This confirms that the travel distance is not affected by these thermal fluctuations, which are dominated by the fluctuations of the starting position of the atomic cloud, before the transport.

This correlation between the top and bottom positions decreases over longer time scales, of hours or days, as can already be observed in figure 5 for timescales of a few thousand seconds. This could actually be

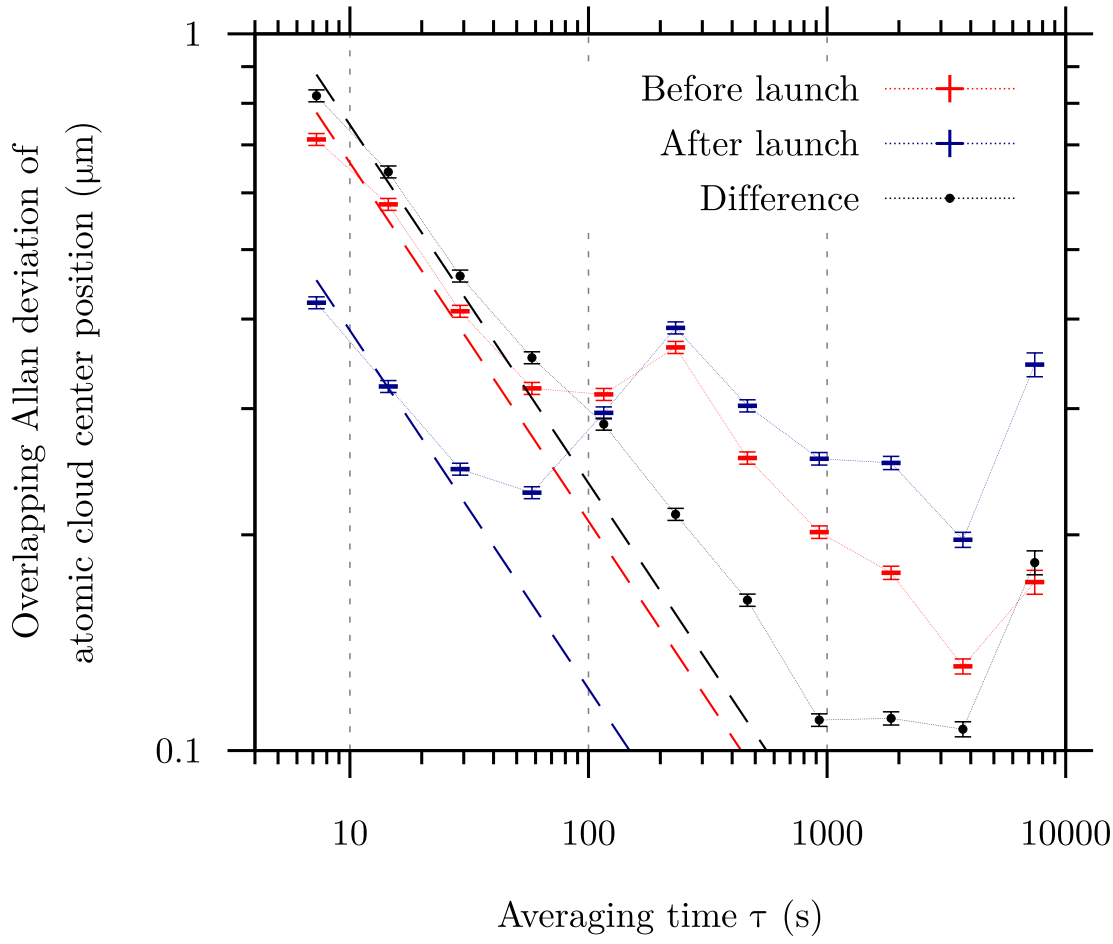

Figure 5. Overlapping Allan standard deviation of the center position of the atomic cloud before and after the transport. For each curve, we plot in dotted lines the $1/\sqrt{\tau}$ decay corresponding to the averaging of white noise, fitted to the first three points.

due to deformations in the mechanical structure supporting our two imaging systems, rather than variations in the actual travel distance.

Finally, the final vertical size of the cloud will determine the spatial resolution of our force sensor. But, given the current resolution of our imaging system of about 9 μm, we are actually not able to precisely determine this size, nor its fluctuations. Nevertheless, since the atoms remain trapped at all times, we expect the size of the atomic cloud to be identical to the size at the end of the evaporation (ie of order of a few micrometers in rms width).

4. Conclusion

We have investigated the efficiency of using Bloch oscillations to transport a cloud of ultracold atoms over a long-range distance of 30 cm, with a precise control of their final position, size and temperature, and with the prerequisites of keeping them trapped at all times. We obtain a maximum efficiency of 25% for their transport, and in the end, we recapture about 10% of the initial number of atoms in the final trap, which combines a blue-detuned static lattice and a red-detuned progressive wave for transverse confinement. Spontaneous emission induces in our setup significant losses and heating, which could be reduced by operating at larger detunings, and thus intensities.

Both the number of atoms and the micrometric spatial resolution of the cloud obtained at the end of our transport process with an optical moving lattice are sufficient for us to move on to measurements of short-range forces between the atoms and the dielectric mirror that retroreflects the lattice beam. In order to integrate these measurements over long periods of time, the stability of the transport is also a prerequisite, which our method fulfills.

Data availability statement

The data that support the findings of this study are available upon reasonable request from the authors.

Acknowledgments

This research has been carried out in the frame of the QuantERA project TAIOL, funded by the European Union's Horizon 2020 Research and Innovation Programme and the Agence Nationale de la Recherche (ANR-18-QUAN-0015-01).

ORCID iD

F Pereira Dos Santos https://orcid.org/0000-0003-0659-5028

References

[1] Peik E, Ben Dahan M, Bouchoule I, Castin Y and Salomon C 1997 Bloch oscillations and an accelerator for cold atoms *Appl. Phys.* B **65** 685–92
[2] Greiner M, Bloch I, Hänsch T W and Esslinger T 2001 Magnetic transport of trapped cold atoms over a large distance *Phys. Rev.* A **63** 031401
[3] Hänsel W, Reichel J, Hommelhoff P and Hänsch T W 2001 Magnetic conveyor belt for transporting and merging trapped atom clouds *Phys. Rev. Lett.* **86** 608–11
[4] Günther A, Kemmler M, Kraft S, Vale C J, Zimmermann C and Fortágh J 2005 Combined chips for atom optics *Phys. Rev.* A **71** 063619
[5] Schwindt P D D, Cornell E A, Kishimoto T, Wang Y-J and Anderson D Z 2005 Efficient loading of a magnetic waveguide on an atom chip *Phys. Rev.* A **72** 023612
[6] Long R, Rom T, Hänsel W, Hänsch T W and Reichel J 2005 Long distance magnetic conveyor for precise positioning of ultracold atoms *Eur. Phys. J.* D **35** 125–33
[7] Pertot D, Greif D, Albert S, Gadway B and Schneble D 2009 Versatile transporter apparatus for experiments with optically trapped Bose–Einstein condensates *J. Phys. B: At. Mol. Opt. Phys.* **42** 215305
[8] Kuhr S, Alt W, Schrader D, Müller M, Gomer V and Meschede D 2001 Deterministic delivery of a single atom *Science* **293** 278–80
[9] Schrader D, Kuhr S, Alt W, Müller M, Gomer V and Meschede D 2001 An optical conveyor belt for single neutral atoms *Appl. Phys.* B **73** 819–24
[10] Middelmann T, Falke S, Lisdat C and Sterr U 2012 Long-range transport of ultracold atoms in a far-detuned one-dimensional optical lattice *New J. Phys.* **14** 073020
[11] Klostermann T, Cabrera C R, von Raven H, Wienand J F, Schweizer C, Bloch I and Aidelsburger M 2022 Fast long-distance transport of cold cesium atoms *Phys. Rev.* A **105** 043319
[12] Unnikrishnan G, Beulenkamp C, Zhang D, Zamarski K P, Landini M and Nägerl H-C 2021 Long distance optical transport of ultracold atoms: a compact setup using a Moiré lens *Rev. Sci. Instrum.* **92** 063205
[13] Lee J H, Jung H, Choi J-Y and Mun J 2020 Transporting cold atoms using an optically compensated zoom lens *Phys. Rev.* A **102** 063106
[14] Couvert A, Kawalec T, Reinaudi G and Guéry-Odelin D 2008 Optimal transport of ultracold atoms in the non-adiabatic regime *Europhys. Lett.* **83** 13001
[15] Alauze X, Bonnin A, Solaro C and Pereira Dos Santos F 2018 A trapped ultracold atom force sensor with a μm-scale spatial resolution *New J. Phys.* **20** 083014
[16] Sorrentino F, Alberti A, Ferrari G, Ivanov V V, Poli N, Schioppo M and Tino G M 2009 Quantum sensor for atom-surface interactions below 10 μm *Phys. Rev.* A **79** 013409
[17] McGuirk J M, Harber D M, Obrecht J M and Cornell E A 2004 Alkali adsorbate polarization on conducting and insulating surfaces probed with Bose-Einstein condensates *Phys. Rev.* A **69** 062905
[18] Ben Dahan M, Peik E, Reichel J, Castin Y and Salomon C 1996 Bloch oscillations of atoms in an optical potential *Phys. Rev. Lett.* **76** 4508–11
[19] Bharucha C F, Madison K W, Morrow P R, Wilkinson S R, Sundaram B and Raizen M G 1997 Observation of atomic tunneling from an accelerating optical potential *Phys. Rev.* A **55** R857–60
[20] Glück M, Kolovsky A R and Korsch H J 1999 Lifetime of Wannier-Stark states *Phys. Rev. Lett.* **83** 891–4